AIP | Journal of Applied Physics

In-situ x-ray diffraction studies on post-deposition vacuum-annealing of ultra-thin iron oxide films

F. Bertram, C. Deiter, K. Pflaum, M. Suendorf, C. Otte et al.

Citation: J. Appl. Phys. **110**, 102208 (2011); doi: 10.1063/1.3661655
View online: http://dx.doi.org/10.1063/1.3661655
View Table of Contents: http://jap.aip.org/resource/1/JAPIAU/v110/i10
Published by the American Institute of Physics.

In-situ x-ray diffraction studies on post-deposition vacuum-annealing of ultra-thin iron oxide films

F. Bertram,[1,a)] C. Deiter,[1] K. Pflaum,[1] M. Suendorf,[2] C. Otte,[2] and J. Wollschläger[2]
[1]*Hamburger Synchrotronstrahlungslabor am Deutschen Elektronen-Synchrotron, Notkestr. 85, 22607 Hamburg, Germany*
[2]*Physics Department, University Osnabrück, Barbarastr. 7, 49069 Osnabrück, Germany*

(Received 1 October 2010; accepted 13 March 2011; published online 30 November 2011)

A maghemite (γ-Fe_2O_3) film of 8.3 nm thickness is epitaxially grown on MgO(001) single crystal substrate by reactive molecular beam epitaxy. Chemical composition and crystal structure of the surface was studied by x-ray photoelectron spectroscopy and low energy electron diffraction, respectively. Afterwards the sample was moved to a heating cell for *in situ* x-ray diffraction experiments on the post-deposition annealing process in high-vacuum to study structural phase transitions of the iron oxide film. The iron oxide film is reduced with increasing temperature. This reduction occurs in two steps that are accompanied by structural transitions. The first step is a reduction from γ-Fe_2O_3 to Fe_3O_4 at 360 °C and the second step is the reduction from Fe_3O_4 to FeO at 410 °C. © *2011 American Institute of Physics*. [doi:10.1063/1.3661655]

I. INTRODUCTION

Iron oxide thin films offer a wide range of possible applications due to their magnetic and catalytic properties. Firstly, they are interesting for the development of room temperature spintronic devices since Fe_3O_4 (magnetite) has a theoretically predicted full spin polarization at the Fermi level and very high Curie temperature of 584 °C.[1] Due to its half metallic character, a possible application for magnetite thin films are magnetic tunnel junctions.[2] Secondly, iron oxide films are also of interest in the field of heterogeneous catalysis like the oxidation of carbon monoxide.[3,4] For both applications a deeper knowledge of the structure and the stability of iron oxide thin films is essential.

In this work we studied the effect of post deposition annealing (PDA) of epitaxial ultra-thin iron oxide films under vacuum conditions. For this purpose we deposited a γ-Fe_2O_3 (maghemite) film on MgO(001) single crystal substrate. MgO forms crystals with rock salt structure and a lattice constant of $a = 4.2117$ Å. Comparing the doubled lattice constant of MgO with the lattice constant of maghemite ($a = 8.3515$ Å) the lattice mismatch is very small (<1%). Due to the similar crystal structure and this very small lattice mismatch between MgO(001) and maghemite the growth of Fe_2O_3 as maghemite is favored versus growth with hematite ($\alpha - Fe_2O_3$) crystal structure.[5,6] Maghemite crystallizes in the cubic defect spinel structure with 32 oxygen anions, $21\frac{1}{3}Fe^{3+}$ cations and $2\frac{2}{3}$ cation vacancies. The oxygen anions form an fcc lattice and 8 cations occupy tetrahedral positions while the remaining cations and the vacancies are randomly distributed among the octahedral cation positions.

The two other iron oxide phases important for this study are Fe_3O_4 (magnetite) and FeO (wüstite). Magnetite crystallizes in inverse spinel structure that is very similar to the maghemite crystal structure. The bulk unit cell has 32 oxygen anions that form an fcc lattice. 8 Fe^{3+} cations occupy tetrahedral positions and the octahedral positions are occupied by 8 Fe^{2+} and 8 Fe^{3+} cations randomly distributed. The magnetite bulk lattice constant ($a = 8.3963$ Å) almost matches the lattice constant of maghemite (lattice mismatch 0.5%).

Wüstite forms a rock salt structure with a lattice constant of $a = 4.332$ Å where both oxygen anions and iron cations form fcc structures, which are shifted by half a lattice constant to each other so that all ions are octahedrally coordinated. Since wüstite is not stable under ambient conditions, it forms a non-stoichiometric iron-deficient phase. It is also important to consider that the symmetry of the oxygen sublattice for these three oxide phases is the same (fcc sublattice). This means that only the iron cations have to rearrange during phase transition of these iron oxide structures.

This study focuses on post deposition annealing of a maghemite ultra-thin film on MgO(001) monitored by *in situ* synchrotron x-ray diffraction (XRD). Prior to the annealing studies, the as-prepared film is studied *in situ* by x-ray photoelectron spectroscopy (XPS) to clarify chemical composition and low energy electron diffraction (LEED) to check crystal quality of the iron oxide surface. After this preliminary characterization x-ray reflectivity (XRR) and XRD measurements were performed to study the film thickness and crystal structure of the as-prepared film.

II. SAMPLE PREPARATION

Sample preparation and film analysis by LEED as well as XPS was performed in a multi chamber ultrahigh vacuum (UHV) system. The base pressure in the preparation chamber is 10^{-8} mbar and 5×10^{-10} mbar in the analysis chamber. For XPS studies a Phoibos HSA 150 hemispherical analyzer (resolution 1 eV) with a SPECS XR-50 x-ray source was used with A1 K_α radiation at 1486.6 eV.

Before deposition the MgO(001) single crystal substrate was cleaned by annealing up to 400 °C in 10^{-4} mbar oxygen

a)Electronic mail: florian.bertram@desy.de.

for 30 min. Afterwards, chemical composition and crystalline quality was checked by XPS and LEED, respectively. XPS shows a chemically clean substrate without carbon contamination and LEED shows clear diffraction spots and cubic symmetry (c.f. Fig. 1(a)). An iron oxide film was grown on the MgO(001) substrate by reactive molecular beam epitaxy (MBE). Pure iron was evaporated by electron beam heating in molecular oxygen atmosphere. During deposition the oxygen partial pressure was kept at 10^{-4} mbar and the substrate temperature was 250 °C. The deposition rate of $0.2\,\text{Å}/\text{s}$ was measured by an oscillating quartz balance calibrated *a posteriori* by XRR. After deposition the sample was cooled in oxygen atmosphere to avoid reduction of the sample. After reaching room temperature the sample was transferred to the analysis chamber for LEED and XPS measurements without breaking UHV conditions. Afterwards the sample was exposed to ambient conditions for the transfer to Deutsches Elektronen-Synchrotron (DESY), Hamburg for XRR and XRD experiments.

III. EXPERIMENTAL SETUP FOR *IN-SITU* X-RAY DIFFRACTION STUDIES

For *in situ* XRD studies a newly developed high vacuum sample cell was used. In this setup the sample is placed on a copper sample stage, which is heated by a resistive heating wire. Temperature is measured by a PT100 temperature sensor mounted to the sample stage.

In this study the sample cell was mounted in horizontal setup at the W1 diffractometer at DESY. The beamline W1 is a wiggler beamline with a Si(111) double crystal monochromator and a six-circle diffractometer. A photon energy of 10.5 keV ($\lambda = 1.18$Å) was used.

To study the effect of annealing in vacuum the sample temperature was stepwise increased using a LakeShore 340 temperature controller. At each step $\theta - 2\theta$ scans were performed close to the MgO $(002)_B$ Bragg peak. Index B denotes the bulk coordinate system. In the following we will use the surface coordinate system for indexing peak positions, which is defined by the MgO(001) surface unit cell. The surface unit cell is half the size of the bulk unit cell in vertical direction and rotated by 45° in lateral direction. Thus, the MgO $(002)_B$ peak is labeled (001) in surface coordinates. (00L) scans were performed close to $L = 1$ where

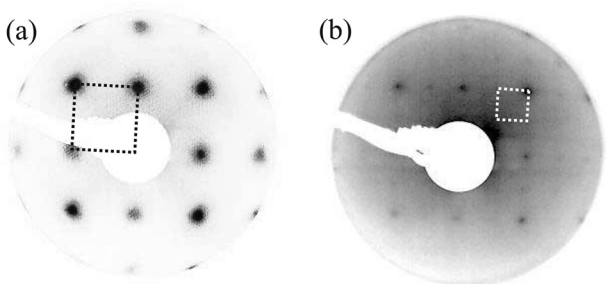

FIG. 1. LEED images of (a) the MgO(001) substrate and (b) the as-prepared film taken at 145 eV electron energy. Both the substrate and the film show clear peaks originating from a cubic unit cell (dashed squares). The spacing between the film diffraction peaks is reduced by a factor of two compared to the substrate peaks indicated a doubled real space lattice constant. Superstructure peaks are visible neither for the substrate nor the film.

FeO, Fe_3O_4, and γ-Fe_2O_3 as well as MgO have Bragg peaks due to constructive interference from the (001) crystal planes. Therefore, this position in reciprocal space is well suited for studying phase transitions between these iron oxide phases. Since thermal expansion is changing the lattice constant of both film and substrate both Bragg peaks are shifting with increasing temperature. Because the thermal expansion coefficient for MgO and iron oxide are almost identical we can use the MgO Bragg reflection as a calibration to compensate the shift caused by thermal expansion.

IV. RESULTS AND DISCUSSION

In the following section the results of our study will be presented. First we will present the analysis of the as-prepared film by LEED, XPS, XRR, and XRD. Afterwards, we will present the results of the *in situ* annealing studies.

A. Sample characterization before the annealing experiment

LEED images (cf. Fig. 1(b)) of the as-prepared film show clear Bragg spots with half peak distance compared to the MgO(001) substrate indicating a doubled lattice constant in real space.

Chambers *et al.*[7] reported this LEED pattern for γ-Fe_2O_3 while an additional $\left(\sqrt{2}\times\sqrt{2}\right)R45°$ structure appears for Fe_3O_4. Therefore, we conclude that the iron oxide film has γ-Fe_2O_3 structure. This result is supported by XPS measurements (cf. Fig. 2). The background corrected Fe2p photoelectron spectrum shows that both the $Fe2p_{1/2}$ peak and the $Fe2p_{3/2}$ have additional satellites (S_0 and S_1), which are shifted by 8 eV to higher binding energies. This structure can be regarded as a fingerprint for the Fe_2O_3 stoichiometry while satellites are not visible for Fe_3O_4[8]. Furthermore, Fujii *et al.*[9] presented detailed multiplet calculations confirming that γ-Fe_2O_3 has these satellites while they are not present for Fe_3O_4. Comparing our spectra with the calculated spectra, the satellite intensities also are in very good agreement with γ-Fe_2O_3 stoichiometry. Thus, combining the results from

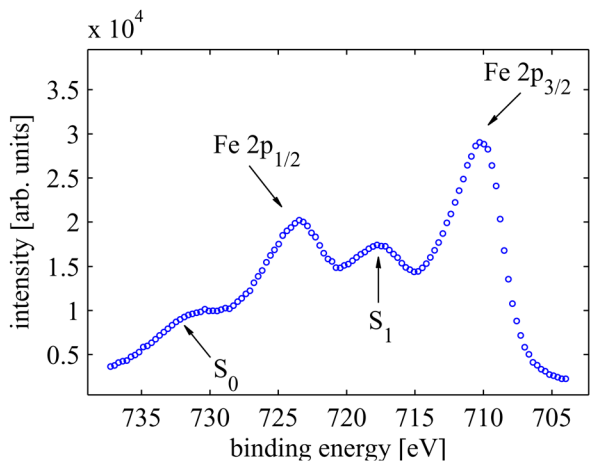

FIG. 2. (Color online) Background corrected XPS measurement of the Fe2p region using a Shirley background. The Fe $2p_{1/2}$ and Fe $2p_{3/2}$ peak structure with satellites S_0 and S_1 shifted by 8 eV indicates complete Fe_2O_3 stoichiometry.

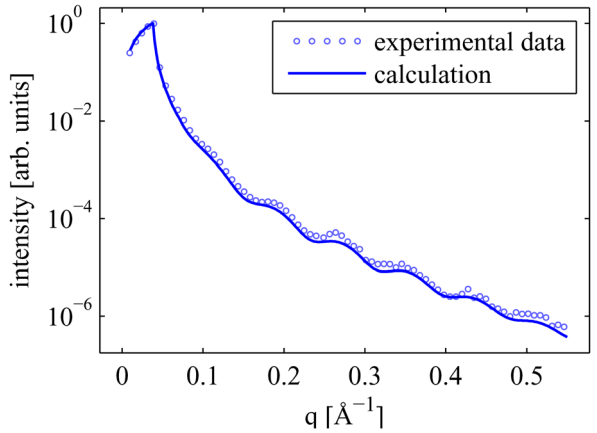

FIG. 3. (Color online) Measured (open circles) and calculated (solid line) x-ray reflectivity intensity before the annealing experiment.

LEED and XPS we can conclude that the as-prepared film is consisting of γ-Fe_2O_3 (maghemite). Since maghemite is known to be stable under ambient conditions, no changes in the sample due to oxidation or reduction are expected during transport.

Figure 3 shows the measured and calculated XRR intensities. The data show clear oscillations due to interference from the scattering at the film/substrate interface and the film surface. From the calculation using the Parratt algorithm with Névot-Croce roughness profile we obtain a film thickness of 8.3 nm for the iron oxide film with 0.2 nm rms surface roughness. The formation of an interface layer between film and substrate cannot be observed by XRR.

Figure 4(a) presents XRD measurements of the (00)-rod close to $L = 1$ and calculated intensity. For calculation kinematic diffraction theory was used. In addition to the sharp peak from the MgO(001) substrate clear oscillations from the iron oxide film are visible. The presence of these oscillations indicates a highly ordered homogeneous film. Since the lattice mismatch between MgO(001) and γ-Fe_2O_3 is very low the sharp Bragg peak of the semi-infinite substrate and Bragg peak broadened due to the finite thickness of the iron oxide film are strongly overlapping, and one has to take into account interference effects.[10] The calculation gives a layer distance of 2.09 Å for the iron oxide film, which is very close to the value for bulk γ-Fe_2O_3 (2.088 Å) supporting the observations by LEED and XPS. Deviations from the bulk value can be explained by strain effects. Since the (doubled) substrate lattice constant is slightly bigger than the γ-Fe_2O_3 bulk unit cell, the film is expanded laterally to fit the substrate lattice. Therefore, the vertical lattice constant is slightly compressed. The interface distance, i.e., the distance between film and substrate in vertical direction, obtained by the calculation is 3.01 Å (1.4 × MgO(001) layer distance).

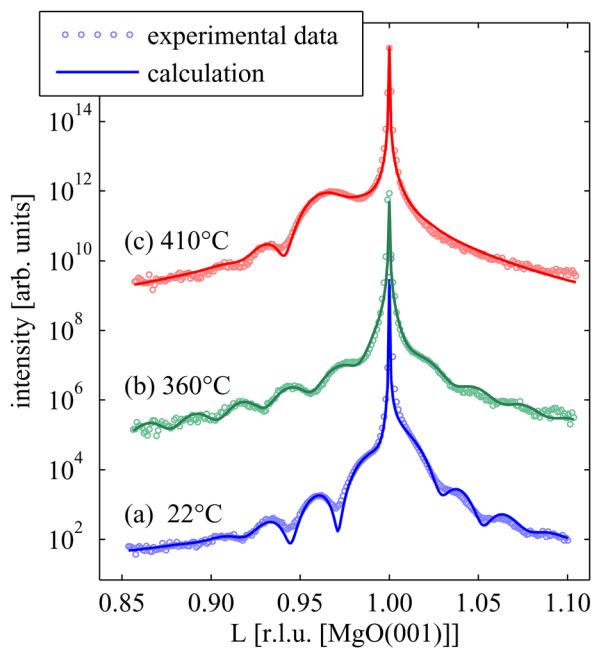

FIG. 4. (Color online) Measured (open circles) and calculated (solid line) XRD intensity before the annealing experiment (a) at $H = K = 0$ and close to $L = 1$, i.e., the $(002)_B$ MgO reflection. In addition the figure shows the measured and calculated intensity at 360°C (b) and 410°C (c) where the phase transition to Fe_3O_4 and γ-Fe_2O_3 are completed.

B. *in situ* sample annealing

Figure 5 presents XRD measurements of the (00*L*) crystal truncation rod (CTR) performed at each temperature step. For all temperatures the measurements show a clear Bragg peak of the MgO(001) substrate. Due to the small lattice mismatch of MgO(001), γ-Fe_2O_3, and Fe_3O_4 the Bragg peaks of film and substrate are strongly overlapping for lower temperatures. For temperatures of 400 °C and higher a clear separation of substrate and film Bragg reflection is observed. For low temperatures clear fringes originated from the iron oxide film are visible, which are attenuated for higher temperatures but recover at specific temperatures. This behavior is illustrated in Fig. 6 showing the evolution of the peak intensity of the fringe of first order appearing at $L \simeq 0.96$ at 22 °C with increasing temperature. Since the fringes are shifting we cannot simply take the intensity at fixed values of L but must follow the gradual shift of the position of the fringe maximum with maximum $\Delta L = 0.03$. Following the fringe intensity a clear decrease can be observed with increasing temperature with two local maxima at 360 °C and 410 °C.

Analyzing the evolution of the vertical layer distance with increasing temperature, an increase in layer distance

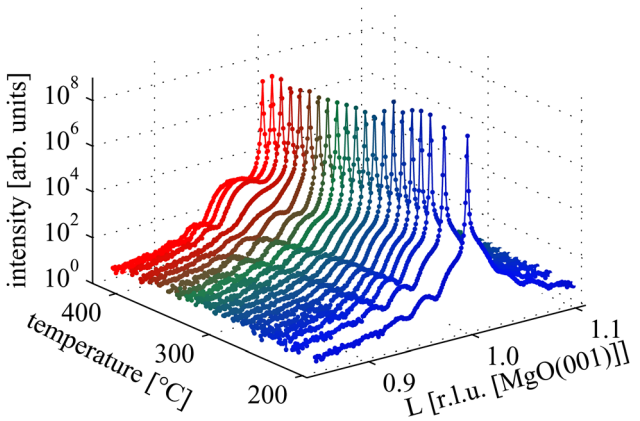

FIG. 5. (Color online) XRD measurements performed at different temperature steps during annealing.

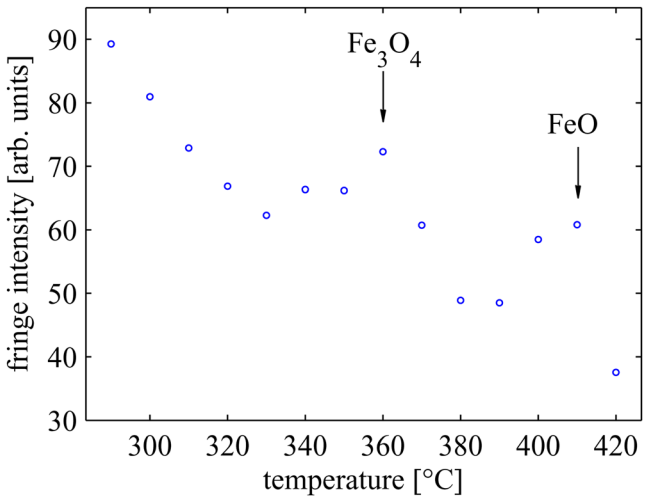

FIG. 6. (Color online) Peak intensity of the first order fringe at $L = 0.96 \rightarrow 0.93$ as a function of temperature.

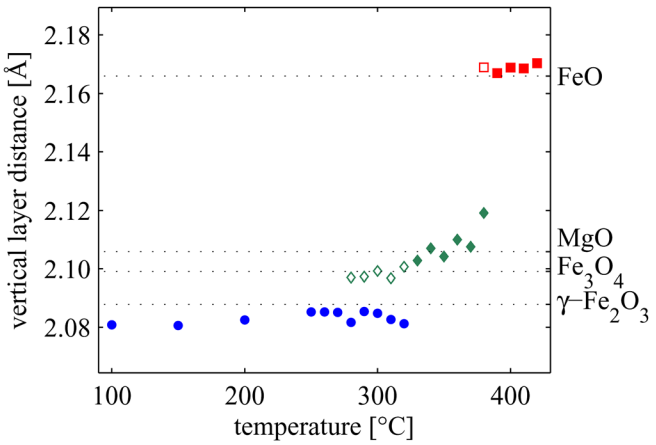

FIG. 7. (Color online) Vertical layer distance of the iron oxide film obtained by XRD corrected for thermal expansion. Blue circles represent the Fe_2O_3, green diamonds the Fe_3O_4, and red squares the FeO phase. In case that two phases are coexisting, the filled symbols represent the majority oxide phase dominating the diffraction pattern and the open symbols represent the minority phase. Dotted lines mark the bulk layer distance of γ-Fe_2O_3 (2.088 Å), Fe_3O_4 (2.099 Å), FeO (2.166 Å), and MgO (2.106 Å).

can be observed. Starting at about 320 °C we observe a shift of the film Bragg peak to lower L values, i.e., the layer distance is increasing, especially close to 390 °C.

For analyzing the XRD measurements, we calculated diffracted intensity using kinematic diffraction theory. For calculations lower than 390 °C, a spinel type unit cell (γ-Fe_2O_3 and Fe_3O_4) was used, while for higher temperatures a rock salt type unit cell (FeO) was used. The vertical lattice constant of spinel type unit cells and rock salt type unit cells are four times the layer distance and twice the layer distance, respectively. We like to emphasize that choosing the proper unit cell type of these two possibilities is not critical for obtaining the vertical layer distance in our full kinematic diffraction calculations. Calculations using only rock salt type unit cells or only spinel type unit cells for all temperatures lead to similar results. Especially, the critical temperatures for phase transitions are not affected. The reason for this is that both lattice structures are very similar. The spinel structure can be regarded as a rock-salt structure with cation deficiencies and partial reordering of the remaining cations. The partial reordering is the reason for the doubled lattice constant. The vertical layer distance of the iron oxide film obtained by these calculations is shown in Fig. 7 as a function of the annealing temperature.

First, we would like to focus on the evolution of the layer distance marked by filled symbols in Fig. 7. Open symbols will be explained below. Starting from a layer distance close to the γ-Fe_2O_3 bulk layer distance, the layer distance increases and reaches an intermediate plateau around 360 °C with layer distance close to Fe_3O_4. Thus, we conclude that we have a phase transition from γ-Fe_2O_3 to Fe_3O_4 completed at this stage. Increasing the temperature to 390 °C, the layer distance increases strongly and reaches a second plateau around 410 °C. Here, the layer distance is close to the FeO bulk value. Therefore, we conclude that the oxide phase changed to FeO. Figure 4 compares measured and calculated intensity at (a) 22 °C (the as-prepared film), (b) 360 °C, and (c) 410 °C to visualize more clearly the shift of the iron oxide Bragg peaks at these temperatures.

As mentioned above, the fringes are slightly damped with increasing temperature indicating a decrease of crystalline order in the film. At about 360 °C the fringes are completely recovering. Thus, the crystalline order in the film has also recovered. The fringes are again lost above 370 °C and recover at about 410 °C.

We attribute this recovering of diffraction intensity to the completion of a phase transition from γ-Fe_2O_3 to Fe_3O_4 at 360 °C and to the completion of the phase transition from Fe_3O_4 to FeO at 410 °C. Both phase transitions are initiated by the loss of lattice oxygen.

The decrease of XRD intensity can be partially attributed to the dynamic Debye-Waller effect, which is proportional to the temperature due to loss of crystalline order. Fringes indicate a film of very homogeneous film thickness, but since the fringes are recovering at some temperatures we do not attribute the loss of fringes to inhomogeneous thickness but to superposition of fringes due to two oxide phases with different vertical lattice constants so that the positions of the fringes of the different oxide phases have anti-phase character and level the diffraction intensity.

This effect is illustrated in Fig. 8 showing the measured and calculated intensity at 290 °C. In addition to the total calculated intensity, the intensity of the single phases is also shown. Comparing the intensity of the single phases, one has to realize that one phase is dominating the summed intensity of both phases by defining the position of the oscillation maxima. This majority phase is marked by filled symbols in Fig. 7 while the minority phase is marked by open symbols.

One has also to mention that the phase transition γ-Fe_2O_3 to Fe_3O_4 appears gradually over a temperature range of about 50 °C with two coexisting phases while the transition from Fe_3O_4 to FeO is more abrupt. These observations can be easily explained by the fact that there is a continuous range of non-stoichiometric bulk phases between γ-Fe_2O_3 and Fe_3O_4 usually labeled $Fe_{3-\delta}O_4$ while there is no continuous range of phases between Fe_3O_4 and FeO.[11]

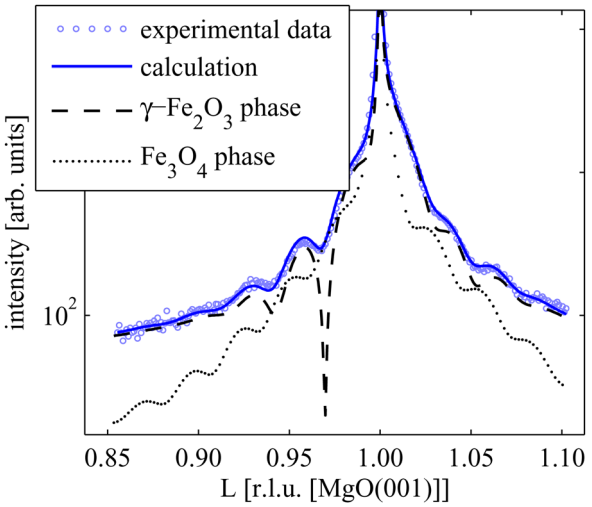

FIG. 8. (Color online) Measured (open circles) and calculated (solid line) diffracted intensity around $L = 1$ at 290°C. The dashed line marks the intensity originated from the majority γ-Fe_2O_3 phase and the dotted line the minority Fe_3O_4.

Combining the observations on the loss of the fringes and the evolution of the vertical layer distance, we conclude that the reduction of the γ-Fe_2O_3 to FeO by annealing in vacuum is occurring in two steps. First, the γ-Fe_2O_3 film is reduced to Fe_3O_4. For the γ-Fe_2O_3 film studied here (thickness 8.3 nm), the critical temperature for this process is 360 °C. The second step is the reduction from Fe_3O_4 to FeO. The critical temperature for this process is 410 °C.

The oxygen partial pressure in the sample cell can be estimated to be roughly 10^{-6} mbar. Assuming this partial pressure together with the phase diagram for bulk iron oxide calculated by Ketteler *et al.*[12] we can conclude the phase transition temperatures expected for bulk iron oxide. The bulk phase transition from Fe_2O_3 to Fe_3O_4 occurs at 780 °C and the Fe_3O_4 to FeO transition at 1200 °C. These values are several 100 °C higher than the values we found in the ultra thin film studied here. We attribute this difference to the small thickness of our film, since reducing the surface to bulk ratio decreases the energy barrier for oxygen desorption into the vacuum. Furthermore, we have to mention that the Fe_2O_3 phase used in the bulk calculations is α–Fe_2O_3 which is the more common and more stable crystal structure for bulk Fe_2O_3. This might be one reason for variations in the critical temperature for the phase transition from γ-Fe_2O_3 to Fe_3O_4 but this cannot explain the smaller critical temperature for the phase transition from the Fe_3O_4 to FeO.

V. CONCLUSION

It was possible to observe the reduction of a γ-Fe_2O_3 ultra thin film epitaxially grown MgO(001) single crystal substrate by monitoring the vertical lattice constant during annealing in high vacuum by *in situ* XRD measurements. The phase transition is accompanied by a reduction of crystalline order in the iron oxide film between two stoichiometric phases. We found that the phase transition is occurring in to steps

$$\gamma\text{-}Fe_2O_3 \overset{360^\circ C}{\rightarrow} Fe_3O_4,$$

$$Fe_3O_4 \overset{410^\circ C}{\rightarrow} FeO.$$

These phase transitions occur several hundred degrees below the values known for the bulk phase transition. We conclude that this change can be attributed to the small film thickness.

ACKNOWLEDGMENTS

We would like to thank W. Calibe for support at beamline W1.

[1] R. J. Harrison and A. Putnis, Am. Mineral. **81**, 375 (1996).
[2] X. W. Li, A. Gupta, G. Xiao, W. Qian, and V. P. Dravid, Appl. Phys. Lett. **73**, 22 (1998).
[3] A. K. Kandalam, B. Chatterjee, S. N. Khanna, B. K. Rao, P. Jena, and B. V. Reddy, Surf. Sci. **601**, 4873 (2007).
[4] S. Wagloehner, D. Reichert, D. Leon-Sorzano, P. Balle, B. Geiger, and S. Kureti, J. Catal. **260**, 305 (2008).
[5] Y. Gao and S. A. Chambers, J. Cryst. Growth **174**, 446 (1997).
[6] Y. Gao, Y. J. Kim, S. Thevuthasan, and S. A. Chambers, J. Appl. Phys. **81**, 3253 (1997).
[7] S. A. Chambers and S. A. Joyce, Surf. Sci. **420**, 111 (1999).
[8] T. Yamashita and P. Hayes, Appl. Surf. Sci. **254**, 8 (2008).
[9] T. Fujii, F. M. F. de Groot, G. A. Sawatzky, F. C. Voogt, T. Hibma, and K. Okada, Phys. Rev. B **59**, 3195 (1999).
[10] T. Weisemoeller, F. Bertram, S. Gevers, C. Deiter, A. Greuling, and J. Wollschläger, Phys. Rev. B **79**, 245422 (2009).
[11] F. C. Voogt, P. J. M. Smulders, G. H. Wijnja, L. Niesen, T. Fujii, M. A. James, and T. Hibma, Phys. Rev. B **63**, 125409 (2001).
[12] G. Ketteler, W. Weiss, W. Ranke, and R. Schlögl, Phys. Chem. Chem. Phys. **3**, 1114 (2001).